INNOVATIVE MECHANICAL ENGINEERING **ISSN 2812-9229 (Online)**
University of Niš, Faculty of Mechanical Engineering
VOL.5, NO 1, 2026, PP. 21-45

Original scientific paper *

DESIGN AND FABRICATION OF A BATTERY-POWERED TRICYCLE FOR SUSTAINABLE URBAN TRANSPORT IN SUB SAHARAN AFRICA

Stanley U. Idi[1], Benjamin U. Oreko[2], Omonigho B. Otanocha[2], Silas O. Okuma[3]

[1]Petroleum Training Institute Effurun, Delta State, Nigeria
[2]Federal University of Petroleum Resources Effurun, Delta State, Nigeria
[3]Maritime University, Okerenkoko, Delta State, Nigeria

Abstract. *Rapid urbanization in Sub-Saharan Africa (SSA) has intensified pressure on existing transport systems, exposing persistent challenges related to accessibility, safety, affordability, and environmental sustainability. Informal mobility modes such as motorcycles and internal combustion engine (ICE) tricycles have expanded rapidly to meet transport demand, but they are associated with high emissions, noise pollution, safety risks, and increasing operational costs. In response to these challenges, this study presents the design, fabrication, analytical evaluation, and experimental testing of a battery-powered electric tricycle developed specifically for urban transport conditions in SSA.A structured engineering design methodology was adopted, encompassing material selection, component fabrication, system assembly, and performance validation. Mild steel was selected as the primary frame material based on a weighted decision matrix considering strength, cost, durability, and manufacturability using locally available fabrication techniques. Analytical design calculations were conducted to estimate power requirements, energy consumption, battery capacity, load distribution, frame bending moments, suspension characteristics, and stability-related parameters. A prototype electric tricycle powered by a 48 V lithium-ion battery and dual 500 W rear hub motors was fabricated and subjected to controlled load, endurance, speed, handling, and braking tests under realistic operating conditions. Experimental results demonstrated that the tricycle safely supported a 100 kg payload without structural deformation, achieved a maximum speed of 60 km/h, and operated continuously for approximately 80 minutes under full-load conditions, exceeding the initial design targets. The findings confirm that the proposed design meets essential performance, safety, and efficiency requirements for short-range urban mobility. This study contributes practical engineering*

*Received: February 14, 2026 / Accepted April 21, 2026.
Corresponding author: Silas O. Okuma
Institution: Maritime university Okerenkoko, Department of Mechanical Engineering, Nigeria
E-mail: silas.okuma@nmu.edu.ng

evidence toward the development of affordable, locally manufacturable electric tricycles and supports their potential role in advancing sustainable intermediate transport solutions in Sub-Saharan Africa.

Key words: *Design and Fabrication, Electric Tricycle, Sustainable Urban Transport, Sub-Saharan Africa Mobility, Battery-Powered Vehicles*

1. INTRODUCTION

Rapid urbanization in Sub-Saharan Africa (SSA) continues to exert significant pressure on existing urban transportation systems, exposing persistent deficiencies in mobility accessibility, operational safety, and environmental quality. Formal motorized transport systems have been unable to scale with urban growth due to high capital requirements, limited route coverage, inflexible scheduling, and inadequate last-mile connectivity [1–3]. As a result, informal and intermediate transport modes—particularly motorcycles and conventional tricycles have emerged as dominant mobility solutions in many SSA cities.

Although these modes address critical transport demand, their rapid and largely unregulated proliferation has introduced substantial technical and societal externalities. Motorcycle taxis and internal combustion engine (ICE) tricycles are associated with high accident rates, excessive noise and exhaust emissions, low energy efficiency, and escalating operational and maintenance costs [9–15]. These challenges are further intensified by increasing urban density, deteriorated road infrastructure, and limited enforcement of vehicle safety standards, collectively undermining urban livability and public health.

Within this context, battery-powered electric tricycles represent a technically viable yet underexplored alternative for sustainable intermediate mobility in SSA [4,5]. Electric tricycles retain the operational flexibility of informal transport while eliminating tailpipe emissions, reducing acoustic pollution, and lowering lifecycle energy and maintenance costs. However, despite increasing market interest in electric two- and three-wheelers across Africa, their engineering suitability for SSA operating conditions—characterized by poor road surfaces, high payload demands, limited charging infrastructure, elevated ambient temperatures, and strong cost sensitivity—remains insufficiently addressed in peer-reviewed engineering literature.

Existing studies on low-carbon mobility in SSA highlight strong latent demand for affordable and sustainable transport solutions but report limited adoption of bicycles and other non-motorized modes due to infrastructure deficits, financial barriers, and weak supply chains [6–8]. Motorcycles have therefore expanded rapidly over the past two decades because of their low entry cost and adaptability to degraded road networks [9], albeit with rising safety risks and adverse public health outcomes [10]. Similarly, ICE tricycles are widely used for passenger and goods transport but suffer from poor fuel efficiency, high emissions, noise pollution, and increasing lifecycle costs [11–14]. With growing concerns related to climate change, urban air quality, and energy security, there is renewed urgency to develop electrified transport solutions that are technically robust, economically viable, and socially inclusive for emerging economies [16,17].

While electric two- and three-wheelers are gradually entering African markets due to their lower operating costs and reduced dependence on fossil fuels [18], most existing publications focus on policy analysis, market penetration, or adoption barriers [19–22].

Consequently, there is a lack of technically rigorous studies that support engineering decisions related to structural frame design, vehicle dynamics, electric powertrain configuration, battery degradation and thermal behavior, and compliance with light electric vehicle testing standards. In particular, empirical evidence addressing the performance of electric tricycles under high dynamic loads, uneven road excitation, and sustained daily operation typical of SSA cities is notably scarce.

The engineering problem addressed in this study is therefore the design and validation of a battery-powered electric tricycle capable of safe, efficient, and affordable operation under SSA urban transport conditions. This problem is defined by multiple quantitative and practical constraints, including the ability to carry combined passenger and cargo loads while maintaining frame structural integrity under repeated dynamic loading, sufficient static and dynamic stability at low-to-moderate urban operating speeds, acceptable energy consumption and driving range per charge under realistic payload conditions, and compatibility with low-cost fabrication methods and informal maintenance ecosystems. Additional constraints include electrical safety, braking performance, and durability consistent with applicable light electric vehicle standards.

The theoretical framework of this work is grounded in sustainable urban mobility, operationalized through an engineering vehicle systems design approach that integrates structural mechanics, vehicle dynamics, ergonomic design, and electric powertrain engineering [23–25]. Prior research demonstrates that tricycle performance is highly sensitive to frame geometry, weight distribution, material selection, and joint integrity [27–30], while ergonomic configuration significantly affects rider comfort, fatigue, and operational safety during prolonged use [31,32]. The adoption of electric propulsion introduces further design considerations, including motor efficiency, battery placement, thermal management, and energy system reliability under high load and temperature variability [33].

The technical novelty of this study lies in the engineering-driven design, fabrication, analytical modeling, and experimental evaluation of a battery-powered electric tricycle explicitly optimized for the transport realities of Sub-Saharan Africa. Unlike existing studies that focus on internal combustion tricycles or provide high-level assessments of electric mobility adoption, this research integrates structural design optimization using locally available and low-cost materials, ergonomic configuration tailored to informal transport use, and a modular electric powertrain architecture designed to accommodate limited charging infrastructure and ease of maintenance. Analytical and numerical models are employed to support key design decisions, including structural stress analysis and energy consumption estimation, prior to fabrication. The prototype is subsequently subjected to experimental testing under realistic operating conditions, with explicit test methodologies, instrumentation, and uncertainty considerations used to evaluate structural performance, energy efficiency, and operational safety.

Despite increasing interest in electric mobility in Africa, there remains a significant gap in engineering-based research documenting the complete design–model–test cycle of electric tricycles tailored to SSA contexts [35,36]. Existing literature rarely reports detailed technical specifications, structural validation, durability assessments, or cost–performance analyses relevant to low-income users and informal transport operators. Addressing this gap, the present study aims to design, manufacture, analytically model, and experimentally evaluate a locally adapted battery-powered electric tricycle that balances safety, affordability, accessibility, and environmental performance. By aligning engineering

design decisions with the operational realities of SSA cities, this work contributes practical, evidence-based insights toward scalable and sustainable intermediate mobility solutions for the region.

2. METHODOLOGY

Utilizing a rigorous methodology (both structurally and mechanically) to construct the battery-powered tricycle resulted in a reliable, safe, and efficient mobility vehicle, meeting both operational expectations and aesthetic appeal. A typical engineering design process was used throughout the development of the tricycle, providing each stage of the project with a precise and orderly method of completion to meet specified functional requirements. All stages of the project were divided into four distinct phases: selecting materials; fabricating the individual components; assembling the overall system; and validating performance. The process utilized a sequential format allowing each stage of the project to inform the subsequent phase, minimizing potential errors; optimizing resource utilization; and ensuring that the completed product met its intended operational requirements.

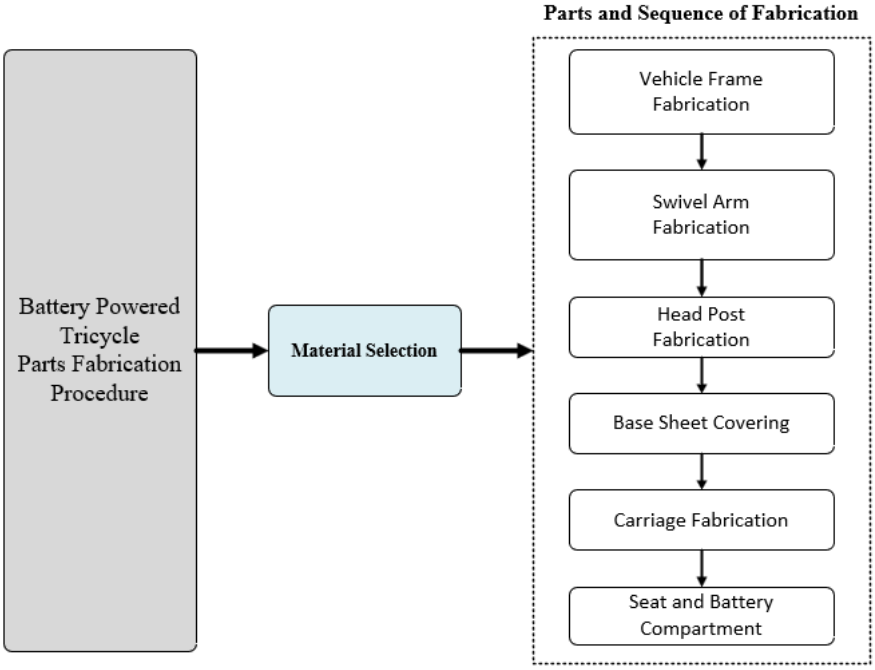

Fig. 1 Sequence of Parts Fabrication

Phase one, Material Selection, emphasized identifying suitable structural and functional materials for the frame of the tricycle, drivetrain, battery enclosure, and electrical components. When considering material selection for the tricycle, key considerations included the strength-to-weight ratio of the material, the material's durability, cost, and how easily the material could be manufactured, ensuring that the tricycle would be both light

and able to support operational loads. In addition to structural properties, materials that could withstand vibration, environmental factors, and electrically generated heat within the system were also evaluated. Phase two, Component Fabrication, entailed converting the selected materials into usable mechanical and electrical components. The mechanical components of the tricycle, including the frame, fork, wheel mounts, and mounting brackets, were cut, formed, welded, or machined to the required dimensional tolerances. While the mechanical components were being fabricated, the electrical components, such as the battery mounting plate, control circuitry enclosure, and wiring harness, were similarly prepared to enable integration during the assembly process. Ensuring high levels of precision during the fabrication process was important to ensure that all components would fit together without issues and function properly over time, regardless of the operating load applied to the system. As depicted in Figure 1, the order in which the parts were fabricated provided a structured workflow that would help minimize production errors and provide consistency in manufacturing quality.

Phase three, System Assembly, consisted of combining all mechanical and electrical components into a single functioning entity. The frame served as the foundation of the tricycle upon which all other components, including the wheels, drivetrain elements, braking system, and electrical modules, are attached. The electric motor and battery pack were mounted to the frame with care to distribute the weight evenly and to manage temperature. Connections between the various electrical components were made so as to avoid interfering with moving parts and to create an interface for the operator to interact with the power delivery system. During this phase, iterative fitting and adjustment were performed to optimize the alignment and functional cohesion of all of the sub-systems.

The fourth and final phase, Performance Validation, consisted of a series of tests designed to evaluate the structural integrity of the tricycle, the reliability of the electrical system, and the operational efficiency of the entire system. Load testing was performed to verify the frames ability to withstand weight and dynamic loads, while electrical diagnostic testing confirmed the motor responded correctly, the battery was performing properly, and the control system was accurate. Finally, road testing was performed to evaluate the tricycles handling, braking, accelerating, and energy consumption over real-world conditions. Any feedback received from these evaluation tests was then used to make any necessary adjustments to the tricycle to improve safety and performance. In conclusion, the systematic and methodical approach taken when designing and constructing the battery powered tricycle guaranteed that it would be built using engineering principles, and therefore possess both functional cohesion and operational dependability. The structured flow of the design process from material selection to performance validation provided a complete work-flow for developing a long-lasting, and efficient, mobility device.

2.1. Material Selection

A systematic decision matrix was used to select the material based on weighted attributes of mild steel, aluminum alloy, and stainless steel such as cost, strength, weight, fabricability, durability and resistance to corrosion. The highest composite rating was realized by mild steel (7.75) which beat aluminum alloy (6.75) and stainless steel (6.65). This resulted in it being the vehicle frame of choice as it was more affordable, weldable and strong enough. The weight and lack of corrosion resistance of mild steel make it

heavier but these shortcomings were deemed to be manageable at the prototype stage with appropriate finishing and reinforcement.

2.2. Parts Fabrication

The fabrication of the bicycle began by creating a detailed computer-aided design (CAD) model. The CAD model allowed for the creation of a detailed design of the main frame, swivel arm, head post, battery housing and carriage assembly. It also allowed for an accurate assessment of the dimensions, tolerance and stress loads of all components. Therefore, it greatly reduced the risk of error during fabrication and ensured that all components could be assembled properly.The main frame of the bicycle was built using mild steel rectangular tubing because it is cost-effective, weldable and has good strength properties. The tubing was cut to length using a bandsaw, then clamped into place using clamping fixtures to align the tubing. Tack welding was then done to hold the tubing in place while full welding was completed to create permanent joints. Once full welding was complete the welds were ground down to a finish. This process created a frame that was structurally sound and provided a solid base for the other sub systems.

Fabricating the swivel arm involved fabricating the individual parts of the arm to the correct radiuses, and then accurately placing the pivot point(s). Jigs were used to ensure that the parts of the swivel arm remained in their correct positions during welding and to help prevent distortion caused by the heat of the weld. Fabricating the swivel arm was critical to the success of the steering mechanism, as the swivel arm is responsible for providing directional control and must have little to no free play and be accurately aligned. To assemble the head post the shaft and the frame tube were machined so that the bearings and locknuts fit properly into the head post. These components were then installed to provide rotationally stable steering and to minimize friction during steering. Then the head post was strengthened using strategically placed welds to protect against the dynamic forces of use. As a result, the head post serves as a durable and mechanically sound steering column.

The bottom covering and carriage assembly were made using 16 gauge steel sheeting and welded to the main structural members of the tricycle. The steel sheeting provided protection for the internal components of the tricycle, and added additional structural stiffness to the tricycle. After welding, surface finishing was done to remove sharp edges and burrs to provide a safe riding environment and to prepare the surfaces for subsequent treatment such as paint or coatings. In addition to providing structural support, the main frame assembly included a bent 16-gauge steel sheet metal configuration to give the tricycle a sleeker look. In addition to the structural support provided by the main frame, the inside of the main frame was insulated and had a circular pipe seat structure made from welded round tubing. The internal reinforcement helped to improve the ergonomics of the ride, distribute the weight of the rider, and improve the overall comfort of the tricycle.Figures 1 – 5 are illustrations of the main frame design, the overall footprint of the tricycle, and the CAD model of the battery-powered tricycle. The figures demonstrate how the structural, ergonomic, and functional aspects of the design are integrated into the fabrication process.

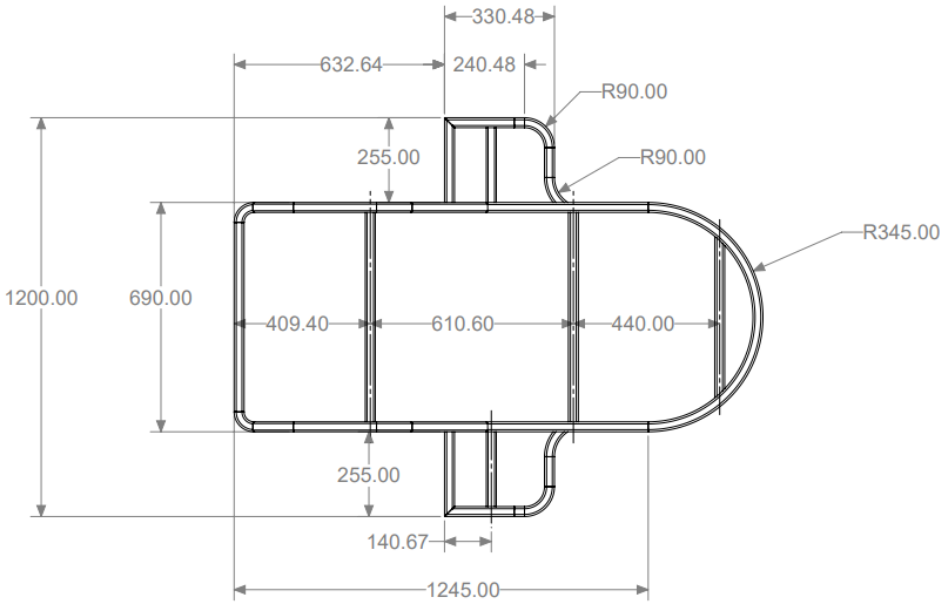

Fig. 2 Main frame dimensions (Top View)

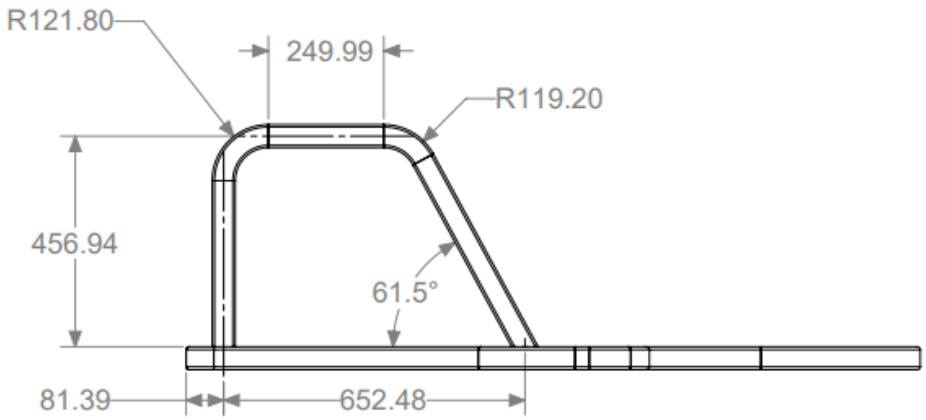

Fig. 3 Main frame dimensions (Side View)

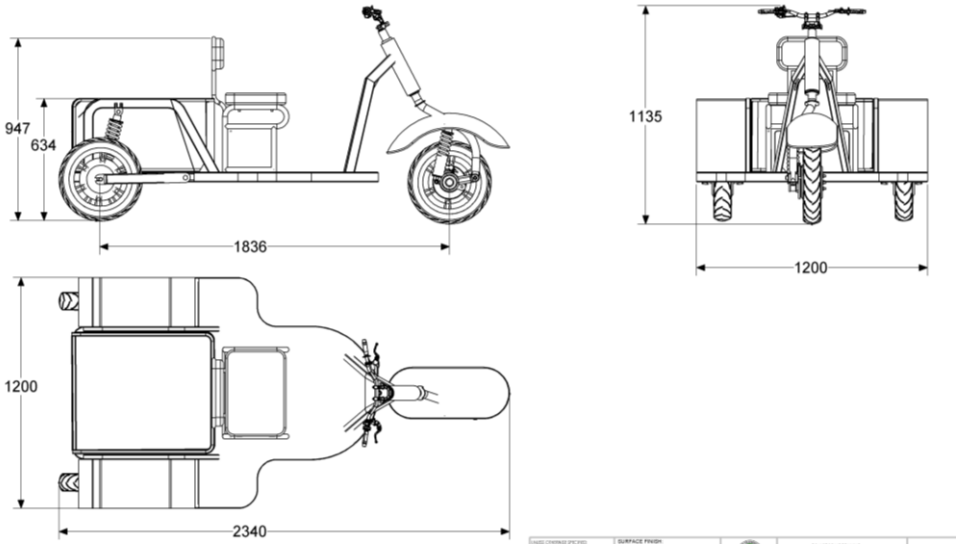

Fig. 4 Footprint/Overall space occupied by the battery powered tricycle

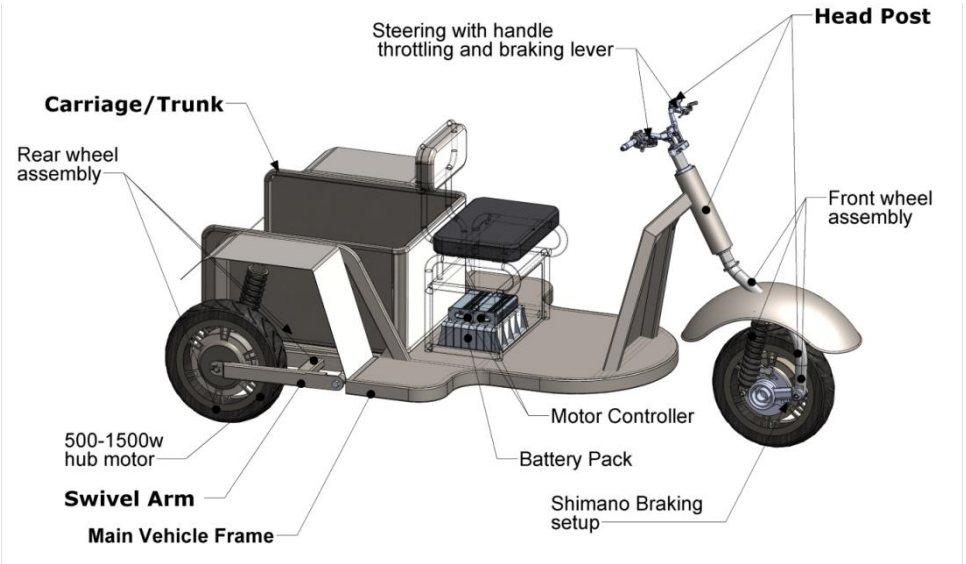

Fig. 5 CAD Model of the battery powered tricycle highlight parts issued for fabrication

2.3. Assembly Procedure and Finishing

The tricycle was assembled in a controlled process of mechanical and electrical assemblies through generating a sequence of aligning structural components to the welded frame by attaching them through torque-controlled fasteners to achieve even weight distributions. This was followed by fitting the motor and the powertrain, i.e. attaching two 500 W hub motors to the rear axle, making sure that it is perfectly aligned to avoid any drift, and also by laying out electrical wiring to allow no heat or mechanical friction. Suspension and wheel systems such as the front fork and two rear rickshaw suspensions were installed and checked to have stable and balanced handling. A lithium-ion battery of 48 V, with built in battery management system was placed below the seat and all the electronic parts such as controller, throttle, display, braking switches and lighting connected and tested over polarity and electrical continuity. The rear trunk and seat assembly was fitted to allow seating comfort to the rider and sufficient load carrying capacity. Lastly, all joints, electrical paths and mechanical interfaces were thoroughly safety checked and then the charging system, motor responsiveness and verification followed, before full operational testing could be done to the fabricated parts.The fabricated parts were prepared by means of filing, grinding, priming, and final painting. The finish enhanced the aesthetic quality, minimized the risk of corrosion as well as guaranteed the durability during the field test.Figure 6-9 show the components and parts fabrication process and assembly [36].

Fig. 6 Testing the fabricated arm with already existing components

Fig. 7 Fabricated head post

Fig. 8 Photo of the first tricycle relevant parts assembling ready for mechanical testing

3. Results and Discussion

3.1. Fabrication Outcomes

The fabrication quality and structural integrity of the tricycle frame and subcomponents were evaluated through dimensional inspection, material verification, and visual weld assessment, with results summarized in Table 1. Mild steel was selected as the primary structural material due to its high yield strength, favorable stiffness-to-cost ratio, good impact resistance, and suitability for welding-based fabrication. These properties are particularly relevant for tricycle operation in SSA environments, where vehicles are subjected to high static payloads, cyclic loading from uneven road surfaces, and occasional impact loading.Steel sheet of gauge 16 (nominal thickness 2 mm) was used for the battery enclosure, carriage panels, and base platform. This thickness provides sufficient bending stiffness and puncture resistance to protect internal components while limiting additional structural mass. The selection balances structural safety and mass efficiency, both of which directly influence vehicle stability and energy consumption. The material's formability and weldability enabled accurate fabrication with minimal residual stresses.

Weld quality was assessed based on bead continuity, penetration, and joint alignment. Across all critical joints, welds exhibited uniform bead geometry and adequate penetration, indicating sound metallurgical bonding. Visual inspection revealed minimal distortion or misalignment, suggesting effective heat control and proper fixturing during welding.

Maintaining weld integrity is critical, as joint failure represents a dominant failure mode in welded vehicle frames subjected to cyclic loading. The observed weld quality therefore supports the frame's ability to withstand operational stresses.

Dimensional inspection of fabricated components showed compliance with the CAD-defined tolerances, allowing assembly without corrective rework. This dimensional accuracy is essential for preserving load paths, ensuring correct alignment of drivetrain and suspension components, and preventing stress concentrations. Overall, the fabrication outcomes demonstrate consistency between the design specifications and the manufactured structure, confirming the suitability of the selected materials, fabrication methods, and quality control procedures [37].

Table 1 Fabrication results

Part	Material Used	Fabrication Method	Observation
Frame	Mild Steel	Welding	Strong, durable; resistant to wear
Battery Compartment	Gauge 16 Steel Sheet	Welding, insulation	Stable, insulated for safety
Load Platform	Mild Steel Frame, Metal Sheet	Welding	Stable, insulated for safety
Seat Frame	Mild Steel tubing	Welding	Comfortable, ergonomic
Motor Mounts and Wheel Assembly	Mild Steel	Welding, alignment	Smooth power transfer, stable

3.2. Assembly Results

Assembly performance was evaluated by assessing component fit-up, alignment, and structural stability during integration, with results summarized in Table 2. The primary frame assembly exhibited no detectable relative movement between joints, indicating adequate geometric stiffness and correct alignment of load-bearing members. This confirms that fabrication tolerances were sufficiently controlled to preserve the intended structural configuration. The battery compartment was installed securely within the frame without interference, ensuring mechanical protection and vibration isolation for the battery system. Proper enclosure alignment is critical to prevent localized stress on battery mounts and electrical connections during operation. Minor misalignments were observed at the rear wheel and hub motor interfaces; however, these were corrected through standard alignment procedures and did not indicate fabrication defects. Ergonomic components including the seat, steering mechanism, and throttle controls were positioned in accordance with the design layout to support rider comfort and intuitive vehicle control. The successful integration of all subsystems demonstrates compatibility between structural, mechanical, and electrical components, resulting in a mechanically stable and test-ready prototype. Figure 9 show the Assembled Product of the Battery Powered Tricycle.

Table 2 Assembly and installation results

Component	Installation Outcome	Observations	Modifications (if any)
Frame Assembly	Secure, stable	Reinforced for durability	None
Battery Compartment	Safely installed, accessible	Insulated and protected	None
Load Platform	Stable, well-aligned	Balanced under full load	None
Motor and Wheels	Aligned, smooth power transfer	Stable during operation	Minor alignment adjustments
Seat Frame and Controls	Comfortable, accessible	Ergonomic control layout	None

Fig. 9 Fully Assembled Product of the Battery Powered Tricycle

3.3. Design Calculations

Table 3 present design specification for electric powered tricycle

Table 3 Assembly and installation results

S/N	Criteria	Specifications
1	Number of wheels	3 wheels
2	Load carrying Capacity	100kg
3	Maximum Operating Speed	50km/hr = 13.89m/s
4	Prime Mover	Electric Hub Motor
5	Number of powered wheels	2 (rear)
6	Powered Source	Battery Electric
7	Chassis Material	Mild Steel
8	Operation Duration on maximum capacity	1hr

3.3.1. Power requirement

The propulsion power required for the electric tricycle was estimated by considering the primary resistive force acting on the vehicle during motion. Since the vehicle is designed to operate at low-to-moderate urban speeds, aerodynamic drag was assumed to be negligible compared with rolling resistance. Therefore, the required propulsion force was estimated based primarily on rolling resistance. The total weight of the vehicle system includes the weight of the tricycle structure, battery system, motors, and the driver. The estimated mass values were obtained from parametric modeling using SolidWorks. The driver mass was assumed as:

$$M_{driver} = 65\text{kg}$$

The corresponding weight is calculated using gravitational acceleration:

$$W = m \times g$$

where, W = weight [N], m = mass [kg] and g = gravitational acceleration [9.81 m/s²]

$$W_{driver} = 65 \times 9.81 = 650\text{N}.$$

The total vehicle weight (including driver and payload) obtained from the parametric model was estimated as:

$$W_{total} = 2317\text{N}.$$

Rolling Resistance Force

The total force required to overcome rolling resistance is expressed as:

$$F_{rr} = C_{rr} \times W$$

where, Frr = rolling resistance force [N], Crr [-] = rolling resistance coefficient (dimensionless) and W = total vehicle weight [N].

Rolling resistance occurs due to deformation of the tires and contact interaction with the road surface. The rolling resistance coefficient depends on tire properties and road conditions. For small utility vehicles operating on paved roads, a typical value of:

$C_{rr} = 0.02$ was adopted, therefore

$F_{rr} = 0.02 \times 2317 = 46.34N$.

Required Propulsion Power

The mechanical power required to overcome the rolling resistance while maintaining constant velocity is given by:

$$P = F \times V$$

where, P = required propulsion power [W], F = rolling resistance force [N], v = vehicle velocity [m/s], The design speed of the vehicle was specified as:

V = 50km/h

Converting to SI unit, $V = \frac{50}{3.6} = 13.89\text{m/s}$.

Thus ,$P = 46.34 \times 13.89 = 643.5W$.

To account for additional uncertainties such as drivetrain losses, road irregularities, and transient loads, a factor of safety (FoS) of 1.5 was applied:

$P_{Design} = 643.5 \times 1.5 = 965.25W$.

Based on the calculated design power requirement, a 1000 W electric motor system was selected due to market availability and standard motor ratings. To improve traction and load distribution, the propulsion system was configured using two rear hub motors, each rated at 500 W, resulting in a combined power output of 1000 W.

This configuration provides sufficient propulsion power for the tricycle while maintaining mechanical simplicity and redundancy in the drive train.

3.3.2. Total Energy Consumption

The energy consumption of the vehicle depends on several factors, including motor power, driving conditions, and overall system efficiency. To estimate the energy required per unit distance travelled (e.g., Wh/km), the relationship between power demand and vehicle speed is used.

$$E_c = \frac{P}{V + \eta}$$

where:

Ec [Wh/km] - energy consumption per unit distance

P = total power output of the motors [W]. In this design, the two hub motors provide a combined power of **1000 W**.

v = average vehicle speed [m/s] or [km/h]

η = overall system efficiency.

The system efficiency (η) accounts for energy losses occurring within the electric propulsion system. These losses arise from, motor electrical and mechanical losses, controller switching losses, drivetrain transmission losses, and auxiliary electrical losses.

For most light electric vehicles, the overall drive train efficiency typically ranges between 0.75 and 0.90 depending on component quality and operating conditions. In this study, a system efficiency value of 0.85 (85%) is adopted to represent realistic operating conditions.

Substituting the design parameters, P=1000W, v=13.89 m/s (corresponding to 50 km/h), η=0.85\eta = 0.85η=0.85 the estimated energy consumption becomes:

$$E_C = \frac{1000}{13.89 \times 0.85}$$

E_C = Energy Consumption=17 [Wh/km]

This calculation provides an approximate estimate of the energy required per unit distance and forms the basis for subsequent battery capacity and range estimations.

$$Energy\ Consumption = 17\ Wh/km.$$

3.3.3. Battery capacity

Given the a known value of maximum power required by the electric (1000W), and the expected operating duration on full capacity (1hr), the battery capacity can be calculated as:

$$Battery\ Capacity = Rated\ Power \times Duration\ of\ operation$$

$$Battery\ Capacity = 1000W \times 1hr = 1000Wh = 1kWh$$

Considering the potential losses in the motor, controller, and drivetrain, a factor safety of 1.5 will be employ it the evaluation above, hence

$$Battery\ Capacity = 1kWh \times 1.5 = 1.5kWh.$$

3.3.4. Estimated Range

The range is the total distance the vehicle can travel on a fully charged battery. This is given as:

$$\text{Range} = \frac{\text{Battery Capacity}}{\text{Energy Consumption}}$$

$$\text{Range} = \frac{1500\text{wh}}{17\text{Wh/km}} = 88.23\text{km}.$$

3.3.5. Load Distribution on Wheels

The vehicle design configuration employs two rear wheels with motors and one idle front wheel for steering. The total weight distributed across the wheels need to be calculated. This is affected by the position of the center of gravity (CoG) and the design geometry.Assume the CoG is closer to the rear wheels (because of the motors and payload in the rear) as seen in the diagram at Figure 10. The load on the rear wheels can be approximated as:

$$W_{rear} = \frac{L_{rear}}{L_{total}} \times W_{total}$$

where:

W_{rear}= total weight supported by both rear wheels

L_{rear}= distance from the CoG to the rear wheels,

L_{total}= total wheelbase (distance from the front wheel to the rear wheels)

W_{total}=Total weight of the vehicle plus payload and driver's weight as computed in section 3.3.1 = 2317N.

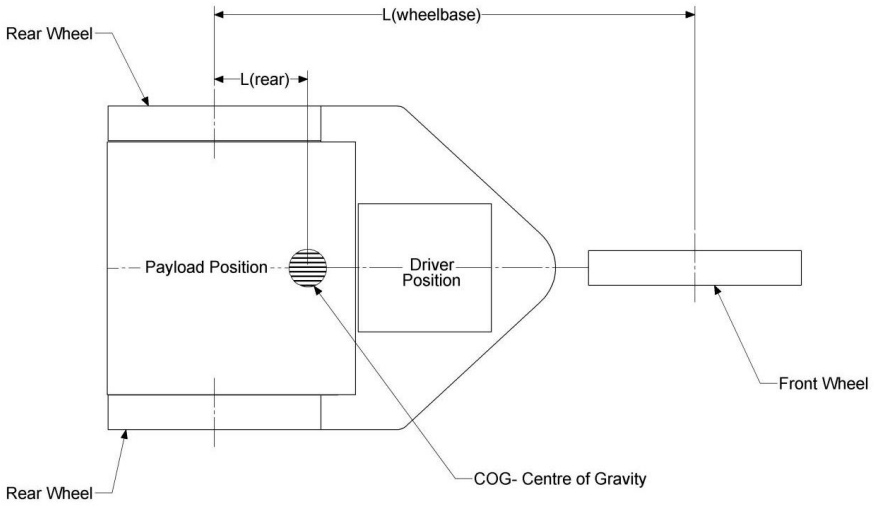

Fig. 10 Diagram showing the position of COG, payload and driver of the vehicle

Where, load on the wheelbase is $L_{wheelbase}$ and load on the rear is L_{rear}
$L_{wheelbase}$=1.836m and L_{rear}=1m.
Hence

$$W_{rear}=\frac{1}{1.836}\times 2{,}317$$

$$W_{rear}=1{,}261.98\text{N}$$

The load on the front idle wheel is:

$$W_{front}=W_{total}-W_{rear}$$

$$W_{front}=2{,}317-1{,}261.98=1{,}055.01\text{N}.$$

3.3.6. Frame Structural Strength: Bending Moment

By simplifying the vehicle as a beam, the frame is modeled as a beam supported at three points: the two rear wheels (assumed to be a single support at the midpoint between them) and the front wheel as shown in Figure 11.

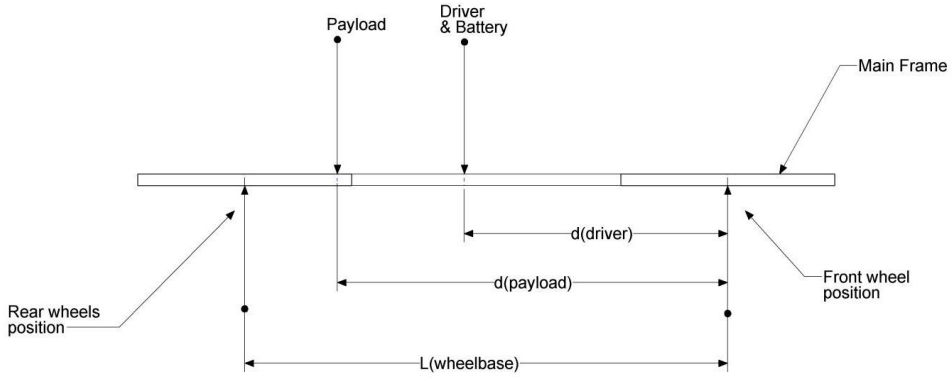

Fig. 11 Simplified Vehicle Loading Diagram

Calculating the Reaction Force at the wheels

Since the rear wheels are located near the payload, they will carry more of the load, while the front wheel supports part of the driver's weight and a portion of the vehicle's own weight.

Let:R_{rear}= be the reaction force at the rear wheels, R_{front}= be the reaction force at the front wheel and W_{total} is total weight

To calculate the reaction forces, we can use the principle of static equilibrium. For the system to be in equilibrium, the sum of forces and the sum of moments about any point must equal zero.

Sum of forces:

$$R_{rear}+R_{front}=W_{total}$$

where W_{total}=2317N.

Sum of Moments:

Taking moments about the rear wheels :

$$R_{front} \times L_{wheelbase} = (W_{payload} \times d_{payload}) + (W_{driver} \times d_{driver})$$

$$R_{front} \times 1.836 = (1000 \times 0.836) + (650 \times 0.6)$$

$$R_{front} \times 1.836 = 1{,}226$$

$$R_{front} = \frac{1{,}226}{1.836}$$

$$R_{front} = 667.76\text{N}.$$

Reaction force at the Rear wheels:

$$R_{rear} = W_{total} + R_{front}$$

$$R_{rear} = 2{,}317 - 667.76$$

$$R_{rear} = 1{,}649.12\text{N}.$$

Bending Moment at key point.

Where M_{mid} moment at the midpoint.

At the midpoint between front and rear wheels: The distance d=1.836/2=0.918m from the front wheel

$$M_{mid} = R_{front} \times 0.918 = 667.76 \times 0.918 = 613\text{Nm}.$$

At the rear wheel: The bending moment at the rear wheels (where the payload is applied) would be the moment due to the driver and part of the vehicle's own weight.

3.3.7. Dynamic Load Considerations

When the vehicle is in motion, additional forces such as dynamic loads and shock loads from road bumps or acceleration must be considered. These can significantly increase the forces acting on the frame. A factor of safety (FoS) of around 1.5 to 2 is typically applied to account for these dynamic forces.

The dynamic load can be estimated by:

$$F_{dynamic} = F_{static} \times FoS$$

Where F_{static} is the static load calculated section 3.3.1 to be 2317N

Hence

$$F_{dynamic} = 2317 \times 1.5$$

$$F_{dynamic} = 3475.5\text{N}.$$

3.3.8. Suspension Design

Suspension design is critical in mitigating shocks from uneven terrain and distributing loads evenly across the wheels. How far the wheel can travel up and down to absorb shocks is refer to a “Wheel travel”. The suspension must allow enough travel to handle the expected load condition.

The wheel travel depends on the vertical deflection:

$$\text{Travel}_{\text{wheel}} = \frac{W_{\text{dynamic}}}{k_{\text{spring}}}$$

where: W_{dynamic}= dynamic load on the wheel, k_{spring}= spring stiffness [N/m].

For better ride comfort, independent suspension was selected for the vehicle design. These means two suspension at the rear (each wheels) and one at the front. See Figure 12 for suspension positions on the conceptual design draft.

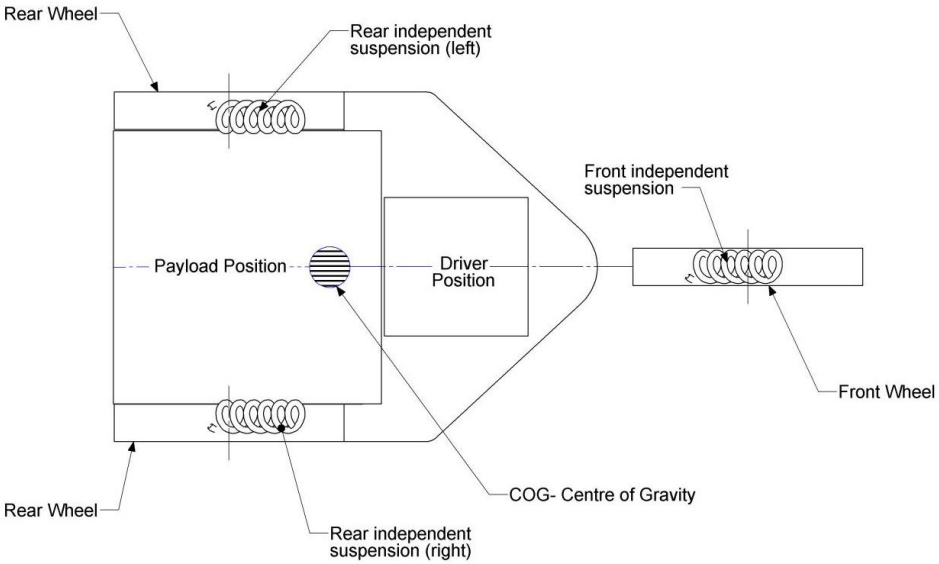

Fig. 12 Suspension positions on the conceptual design draft

Considering the terrain of driving the vehicle, the maximum height of bumps is 100mm (0.1m). A Wheel travel value of half of this value is considered moderate for ride comfort (i.e 50mm=0.05m). Hence

$$k_{\text{spring}} = \frac{W_{\text{dynamic}}}{\text{Travel}_{\text{wheel}}}$$

$$k_{\text{spring}} = \frac{3{,}475.5\text{N}}{0.05\text{m}}$$

$$k_{\text{spring}} = 69{,}510\text{N/m}.$$

The total weight, W_{total}[N] will now be distributed as:

Two rear suspensions (one for each rear wheel) sharing the load at the back.

One front suspension supporting the load at the front.

Since the vehicle is symmetric, each rear suspension should bear half the load carried by the rear.

The ratio of weight at the rear to the weight of the vehicle (fully loaded) is

$$\text{Rear}_{\text{weight ratio}} = \frac{W_{\text{rear}}}{W_{\text{total}}} = \frac{1{,}261.98}{2{,}317} = 0.53$$

The get the required spring constant at the rear $k_{spring\ rear}$ we have:

$$k_{spring\ rear}=k_{spring}\times Rear_{weight\ ratio}$$

$$k_{spring\ rear}=69{,}510\times 0.53=36{,}840.3\text{N/m}.$$

Since the rear has two suspensions, each suspension is expected to have:

$$k_{spring\ each\ rear}=\frac{k_{spring\ rear}}{2}=\frac{36{,}840.3}{2}=18{,}420.15\text{N/m}.$$

The get the required spring constant at the front wheel $k_{spring\ front}$ we have:

$$k_{spring\ front}=k_{spring}\times (1-Rear_{weight\ ratio})$$

$$k_{spring\ front}=69{,}510\times(1-0.53)=32{,}669.7\text{N/m}.$$

Effective Spring Rate Based on Angle

An inclined suspension allows for a longer effective suspension travel distance, which can improve the vehicle's ability to absorb shocks from uneven terrain. This results in better ride comfort. Inclining the suspension often helps to lower the height of the mounting point, thereby lowering the vehicle's center of gravity. A lower center of gravity improves stability during cornering and handling.

When the suspension is inclined, the effective force acting on the spring will be reduced by a factor based on the angle θ between the vertical axis and the suspension

The effective spring rate k_{eff} is calculated as:

$$k_{eff}=k_{spring\ each\ rear}\times \cos\theta$$

where: $k_{spring\ each\ rear}$= spring constant of each rear suspension = 18,420.15N/m, θ= angle of inclination of the suspension from vertical. (30^o)

Hence

$$k_{eff}=18{,}420.15\times \cos 30=15{,}952.32\text{N/m}$$

It can deduced from equation x that as the angle increases, the suspension becomes softer because less of the force is directly in line with the spring. The inclination angle θ is a design trade-off. Too steep an angle will reduce the effective spring rate too much, causing the suspension to be too soft. On the other hand, too shallow an angle may not provide enough suspension travel. Typically, angles between 30° and 45° are chosen for rear suspensions in small vehicles.

Effective Suspension Travel:

The effective vertical suspension travel $T_{eff\ vertical}$ which is a function of the wheel travel $Travel_{wheel}$ will also change based on the angle of the suspension.

$$T_{eff\ vertical}=Travel_{wheel}\times \cos\theta$$

Where:$T_{eff\ vertical}$= effective vertical travel of the wheel, $Travel_{wheel}$= actual travel of the spring (50mm=0.05m)

Hence

$$T_{eff\ vertical}=0.05\times \cos 30=0.043\text{m (43mm)}.$$

Effective Force Distribution on the Rear Region of the Frame

The force transmitted to the rear part of the frame changes with the angle. The component of force acting along the spring's axis F_{spring} is related to the vertical load W_{rear} at the rear:

$$F_{spring.rear}=\frac{W_{rear}}{\cos\theta}$$

where:

$F_{spring.rear}$= force acting along the spring's axis at the rear

Hence

$$F_{spring.rear}=\frac{1{,}261.98}{\cos 30}=1{,}457.21\text{N}.$$

3.3.9. Swingarm Calculation

The swingarm carrying the wheel will affect how much leverage it applies to the suspension. A longer swingarm applies more leverage to the spring, allowing it to absorb shocks more gradually. The leverage ratio for the swingarm design is given as:

$$Leverage\ Ratio=\frac{L_{swingarm}}{L_{suspention}}$$

where:

$L_{swingarm}$= distance from the swingarm pivot to the rear wheel (see Figure 4)

$L_{suspention}$= distance from the swingarm pivot to the point where the suspension is mounted. (see **Fig.13**)

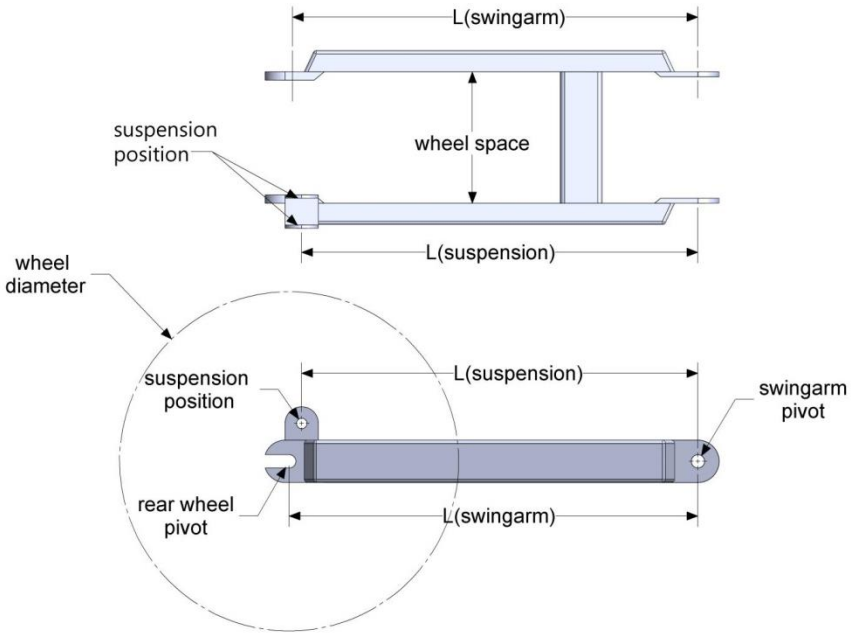

Fig. 13 Swingarm details

Using a 16inch wheels and swingarm as accommodating as possible (moderate), the value for $L_{swingarm}$ and $L_{suspention}$ gives 490mm and 475mm respectively. Hence:

$$Leverage\ Ratio = \frac{490}{475} = 1.03.$$

Deduction: A leverage ratio of 1.03 means that the suspension linkage or swingarm is providing a slight mechanical advantage in transmitting the wheel's motion to the suspension (spring or damper). Specifically, it implies that for every 1 unit of travel at the wheel (or swingarm), the suspension spring or damper will compress or move 1.03 units

3.3.10. Camber Angle Calculation

Camber refers to the angle of the wheels relative to the vertical axis when viewed from the front or rear of a vehicle. It can be either positive camber (wheels tilt outward at the top) or negative camber (wheels tilt inward at the top). The camber angle is given as:

$$\theta = \tan^{-1}\left(\frac{\text{Offset}}{\text{Wheel Height}}\right)$$

where:

θ= Camber angle

Offset= Horizontal displacement between the top and bottom of the wheel (i.e., the distance the top of the wheel is tilted inward or outward)(0mm),

Wheel Height= The vertical distance between the ground and the top of the tire (433.61mm) see **Fig. 14**.

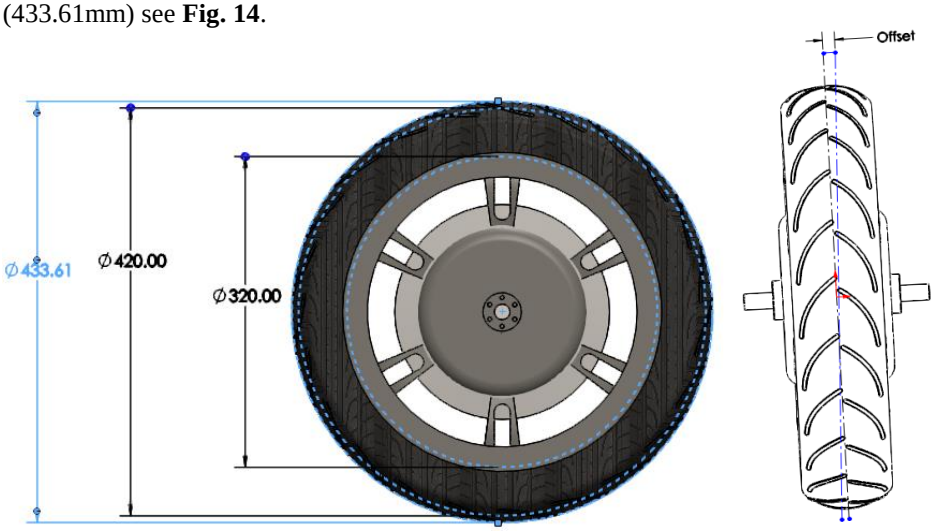

Fig. 14 Selected Wheel Dimensions

Since the vehicle is designed for load transport rather than high-performance cornering, a 0° camber is prepared as it's a good choice to prevent excessive tire wear and ensure longer tire life. This also minimizes the frequency and cost of tire replacements. This implies the offset is 0 as no horizontal displacement between the top and bottom of the wheel.

Hence

$$\theta = \tan^{-1}\left(\frac{0}{433.61}\right) = 0^0$$

Deductions:

A 0° camber angle ensures that the entire width of the tire maintains consistent contact with the road surface during straight driving. This is particularly important for a vehicle designed to carry loads, as it maximizes traction and load distribution across the tire surface. For a utility vehicle that will be carrying heavy payloads and workshop equipment, having maximum tire contact can improve stability and reduce the risk of uneven tire wear under heavy loads. Negative or positive camber causes the tires to wear more on the inner or outer edges, respectively.

3.4. Performance Testing

Performance evaluation was conducted through controlled experimental tests focusing on speed capability, load carrying capacity, endurance, handling, and braking behavior. The measured maximum speed of 60 km/h exceeded the design target of 50 km/h. This result can be analytically justified by considering the total propulsion power available from the dual rear hub motors. The tricycle employs two 500 W hub motors operating at 48 V, providing a combined rated mechanical power of approximately 1 kW. Under steady-state conditions on level ground, the maximum speed is governed by the balance between propulsion power and resistive forces, primarily rolling resistance and aerodynamic drag. Given the relatively low frontal area and operating speeds typical of urban conditions, the measured speed falls within a physically plausible range for the installed powertrain.

Load testing was conducted with a payload of 100 kg to simulate combined passenger and cargo conditions. No permanent deformation, instability, or degradation in handling was observed during testing, indicating that the frame stiffness and strength were sufficient to support the applied loads. This outcome is consistent with the structural design assumptions and material selection. Endurance testing evaluated the operational duration of the 48 V lithium-ion battery system under full-load conditions. The measured continuous operation time of 80 minutes exceeded the predicted one-hour target. From an energy perspective, endurance is governed by the usable battery capacity and average power demand. The extended operating time suggests that the average power draw during testing was lower than the combined rated motor power, which is expected under partial-load urban driving conditions.

Braking performance was assessed through repeated deceleration tests under load. The tricycle exhibited stable braking behavior with no wheel lock-up or lateral instability. Although detailed stopping-distance measurements were not recorded, the absence of skidding indicates adequate brake force distribution and sufficient tire-road friction. Steering responsiveness remained consistent between unloaded and fully loaded conditions, indicating acceptable weight distribution and steering geometry. Overall, the experimental results, supported by simplified physical reasoning, confirm that the prototype meets the intended performance criteria for short-range urban transport applications typical of Nigeria and other SSA regions [38].

3.4. Market Feasibility and Adoption Barriers

Market feasibility analysis indicates that the battery-powered tricycle offers clear operational cost advantages over ICE tricycles by eliminating fuel consumption and reducing routine maintenance requirements. These benefits are particularly significant for informal transport operators who are highly sensitive to fuel price volatility and maintenance downtime. Over the vehicle lifecycle, lower energy and servicing costs are expected to offset higher upfront capital costs.However, several adoption barriers were identified. The cost of key components particularly electric motors, lithium-ion batteries, and power electronics remains significantly higher than that of conventional ICE systems, limiting affordability for many users. In addition, charging infrastructure is limited across many urban and peri-urban areas in SSA, and unreliable grid power further constrains widespread adoption. Battery replacement costs and inconsistent availability in local markets also pose challenges. Furthermore, limited user familiarity with electric vehicles highlights the need for targeted training programs, policy incentives, and supportive regulatory frameworks to facilitate adoption [39–41].

4. CONCLUSION

This study presented the engineering design, fabrication, analytical assessment, and experimental validation of a battery-powered electric tricycle tailored to the operational realities of urban transport in Sub-Saharan Africa. A structured design methodology was employed to ensure that material selection, structural configuration, powertrain sizing, and suspension layout were compatible with high payload demands, uneven road conditions, limited maintenance infrastructure, and strong cost sensitivity typical of informal transport systems in the region.

Analytical calculations were used to guide key design decisions, including motor power selection, battery capacity sizing, load distribution, frame bending behavior, and suspension stiffness. Mild steel emerged as the most suitable frame material due to its favorable strength-to-cost ratio, weldability, and local availability, enabling fabrication using conventional workshop tools. The integration of a 48 V lithium-ion battery system with dual rear hub motors provided adequate propulsion while maintaining mechanical simplicity and modularity. Experimental testing confirmed that the fabricated prototype met or exceeded its design targets. The tricycle demonstrated stable structural performance under a 100 kg payload, achieved a maximum speed of 60 km/h, and delivered an endurance of approximately 80 minutes under full-load conditions. Braking and handling performance remained stable during testing, indicating acceptable weight distribution and steering geometry for low-to-moderate urban operating speeds. These results validate the suitability of the proposed design for short-distance passenger and goods transport applications common in SSA cities.

While the study establishes the technical feasibility of a locally fabricated electric tricycle, certain limitations remain. Advanced numerical simulations, detailed battery thermal and degradation analysis, standardized braking-distance measurements, and long-term durability testing were beyond the scope of this work. Future research will address these aspects, alongside control system optimization, life-cycle cost assessment, and field trials involving extended daily operation.

Overall, this research provides practical, engineering-based evidence supporting the viability of battery-powered electric tricycles as a sustainable intermediate mobility solution for Sub-Saharan Africa. By aligning design choices with regional constraints and operational needs, the study contributes toward scalable, low-emission, and economically accessible urban transport alternatives.

REFERENCES

1. Akinsade, A., Eiche, J. F., Akinola, A. O., & Famodun, M. O. (2023). *Conceptual design and analysis of a tricycle mounted solar-powered photovoltaic cold room system*. Nigerian Journal of Technology, 42(4), 457-463.
2. Almansour, M. (2022). Electric vehicles (EV) and sustainability: Consumer response to twin transition, the role of e-businesses and digital marketing. Technology in Society, 71, 102135.
3. Dodoo, J. E., Dankyi, L. A., & Dankyi, J. K. (2025). Exploring narratives on the factors explaining the use of tricycles for commercial transportation, and leading indicators for road safety in Ghana. African Transport Studies, 3, 100020.
4. Guarnieri, M. (2011). *When cars went electric, part 2 [historical]*. IEEE Industrial Electronics Magazine, 5(2), 46-53.
5. Hofman, I., Sergeant, P., Van den Bossche, A., Koroglu, S., & Kesler, S. (2015). *Integrated model of power electronics, electric motor, and gearbox for a light EV*. Journal of Power Electronics, 15(6), 1640-1653.
6. Hopkins, E., Potoglou, D., Orford, S., & Cipcigan, L. (2023). *Can the equitable roll out of electric vehicle charging infrastructure be achieved?*. Renewable and Sustainable Energy Reviews, 182, 113398.
7. Mensah, E., Ebong, O., Ayeni, Q., & Eze, F. (2023). *Women as public transport providers: a qualitative study of the perception of female tricycle riders in Nigeria*. Journal of Population and Social Studies [JPSS], 31, 832-848.
8. Mensah, E. O., Nyong, B. O., Mensah, E. O., & Ayeni, Q. O. (2025). *When tricycles speak: Language practices and ideology in tricycle texts in Nigeria*. Journal of Asian and African Studies, 60(3), 1724-1738.
9. Ong, A. K. S., Prasetyo, Y. T., Lagura, F. C., Ramos, R. N., Sigua, K. M., Villas, J. A., ... & Diaz, J. F. T. (2023). *Determining tricycle service quality and satisfaction in the Philippine urban areas: A SERVQUAL approach*. Cities, 137, 104339.
10. Jansson, A., Söderling, F., & Söderling, F. (2024). Providing Women with Technology in Rural Areas of Sub-Saharan Africa A case study exploring the acceptance, usage, and effects of Electric Tricycles among Rural Women in Zimbabwe.
11. Yange, T. S., Onyekwere, O., Rufai, M. A., Egbunu, C. O., & Ogboli, O. R. (2020). *Determination of the Severity of Motorcycle and Tricycle Accidents in Nigeria*. Pdfs. Semanticscholar. Org. https://doi. org/10.11648/j. aas, 2020050(2.14), 5.
12. Sebwa, O. S., Chombo, P. V., Gerutu, G. B., Kivugo, R. O., Hosea, J. H., & Greyson, K. A. (2025). *Energy, Economy and Environmental Assessment of E-Tricycle for Medium-Size Cargo Deliveries: A Case of Dar es Salaam City*. The Journal of Engineering, 2025(1), e70073.
13. Veza, I., Asy'ari, M. Z., Idris, M., Epin, V., Fattah, I. R., & Spraggon, M. (2023). Electric vehicle (EV) and driving towards sustainability: Comparison between EV, HEV, PHEV, and ICE vehicles to achieve net zero emissions by 2050 from EV. Alexandria Engineering Journal, 82, 459-467.
14. Vuddanti, S., Shastri, S., & Salkuti, S. R. (2022). Design of permanent magnet brushless DC motor for electric vehicle traction application. In Recent Advances in Power Electronics and Drives. Select Proceedings of EPREC 2021 (pp. 317-333). Singapore: Springer Nature Singapore.
15. Oluwakoya, A. O. (2024). A comprehensive assessment of transportation emissions in Nigeria: Trends, drivers, and impacts. Proceedings of the Nigerian Academy of Science, 16(1s), 61-71.
16. Okeke, F. O., Okosun, A. E., Udeh, C. A., & Okekeogbu, C. J. (2020). Cities for People: the dependency & Impact of Automobile in the Life of City dwellers. European Journal of Sustainable Development, 9(3), 157-157.
17. Farquharson, D. T. (2019). Sustainable energy transitions in sub-Saharan Africa: impacts on air quality, economics, and fuel consumption. Carnegie Mellon University.

18. Ayetor, G. K., Mbonigaba, I., & Mashele, J. (2023). *Feasibility of electric two and three-wheelers in Africa*. Green Energy and Intelligent Transportation, 2(4), 100106.
19. Opiyo, R., & Njenga, P. (2023). Transitioning to Electric Mobility: Low Hanging Fruits in the Two and Three-Wheeler Public Transport Market in Kenya. European Business Law Review, 34(1).
20. Collett, K. A., Byamukama, M., Crozier, C., & McCulloch, M. (2020). *Energy and transport in Africa and South Asia*. Energy Econ Growth.
21. Khan, T., Kohli, S., Yang, Z., & Miller, J. (2022). *Zero-emission vehicle deployment: Africa*. International Council on Clean Transportation.
22. Etukudoh, E. A., Usman, F. O., Ilojianya, V. I., Daudu, C. D., Umoh, A. A., & Ibekwe, K. I. (2024). *Mechanical engineering in automotive innovation: A review of electric vehicles and future trends*. International Journal of Science and Research Archive, 11(1), 579-589.
23. Leal Filho, W., Abubakar, I. R., Kotter, R., Grindsted, T. S., Balogun, A. L., Salvia, A. L., ... & Wolf, F. (2021). *Framing electric mobility for urban sustainability in a circular economy context: An overview of the literature*. Sustainability, 13(14), 7786.
24. Anthony Jnr, B. (2025). Sustainable mobility governance in smart cities for urban policy development–a scoping review and conceptual model. Smart and sustainable built environment, 14(3), 649-671.
25. Musida, M., Hanafi, I., & Sukardjo, M. (2025). Electric Vehicle Shared Services: A Decade of Innovation, Challenges, and Transformative Impact on Sustainable Urban Mobility—A Systematic Literature Review. The Open Transportation Journal, 19(1).
26. Nedjalkov, A., Meyer, J., Göken, H., Reimer, M. V., & Schade, W. (2019). Blueprint and implementation of rural stand-alone power grids with second-life lithium ion vehicle traction battery systems for resilient energy supply of tropical or remote regions. Materials, 12(16), 2642
27. Peiris, K., Senanayake, V., & Sumanarathne, J. (2022). Design Analysis of a Human Powered Tricycle to Introduce Tricycle Culture for Reducing Fossil Fuel in Transportation. NERS 2022, 1.
28. Kubde, A. S., Mehta, G. D., & Tembhurkar, C. K. (2020). *Design Of Human Powered Vehicle: A Concept*. International Journal of Innovations in Engineering and Science, 5, 10-25.
29. Youssef, H. A., El-Hofy, H. A., & Ahmed, M. H. (2023). *Manufacturing technology: materials, processes, and equipment*. Crc Press.
30. Yan, L., & Xu, H. (2025). Lightweight composite materials in automotive engineering: State-of-the-art and future trends. Alexandria Engineering Journal, 118, 1-10.
31. Musa, A. I. (2024). *Optimizing Tricycle Workstations: A Study on Rider Comfort and Ergonomic Solutions*. Acta Technica Corviniensis-Bulletin of Engineering, 17(1), 113-117.
32. Too, D., & Landwer, G. E. (2000). The effect of pedal crank arm length on joint angle and power production in upright cycle ergometry. Journal of sports sciences, 18(3), 153-161.
33. Weinert, J., Ma, C., & Cherry, C. (2007). The transition to electric bikes in China: history and key reasons for rapid growth. Transportation, 34(3), 301-318.
34. Wilson, D. G., & Schmidt, T. (2020). *Bicycling science*. MIT press.
35. Agaton, C. B., Collera, A. A., & Guno, C. S. (2020). Socio-economic and environmental analyses of sustainable public transport in the Philippines. Sustainability, 12(11), 4720.
36. du Tsala, A. A., Adam, S. U., Shittu, A. I., Ado, H. A., & Ibrahim, A. U. (2023). *Solar powered tricycles in Maiduguri: exploring sustainable urban mobility through contingent valuation method*. Ilorin Journal of Economic Policy, 10(2), 16-31.
37. Rastoder, E., Petralia, M. S., Sutton, F. D., & Neumann, J. T. (2020). *Adapted Tricycle*.
38. Dutta, P. P., Dutta, P. P., & Baruah, M. G. (2023). *Design, Development and Analysis of an Improved Tricycle*. In Sustainable Material, Design, and Process (pp. 41-77). CRC Press.
39. Thangavel, S., Narendran, J., Logesh, P., Kabilan, S., & Praveen, D. (2025). *Integrated Structural and Drivetrain Engineering for Enhanced Efficiency in Electric Three-Wheel Freight Vehicles*. Journal of Thermal and Sustainable Energy Systems, 1(1), 1-12.
40. Samuel, B., & Okuma, O. S. (2021). *Design and simulation analysis of cowpea dehulling Machine*. Global Journal of Engineering and Technology Advances, 7(02), 050-066.
41. Okuma, O. S., & Chidi, I. G. (2022). Design and construction of a racing go-kart: The braking system.